Nano- and microstructural evolution of alginate beads in simulated gastrointestinal fluids. Impact of M/G ratio, molecular weight and pH

Laura G. Gómez-Mascaraque[1*], Marta Martínez-Sanz[2], Sean A. Hogan[1], Amparo López-Rubio[2], André Brodkorb[1]

[1] Teagasc Food Research Centre, Moorepark, Fermoy, Co. Cork, Ireland

[2] Food Safety and Preservation Department, IATA-CSIC, Avda. Agustin Escardino 7, 46980 Paterna, Valencia (Spain).

*Corresponding author: Tel.: +353 76 111 22 41

E-mail address: laura.mascaraque@teagasc.ie (L. G. Gómez-Mascaraque)[1]

[1] Abbreviations: G, α-L-guluronic acid; M, β-D-mannuronic acid; HPLC-SEC, High performance size exclusion chromatography; SAXS, small angle X-ray scattering; SGF, simulated gastric fluid; SIF, simulated intestinal fluid

ABSTRACT

Alginate microcapsules were prepared using three different alginate grades and incubated under simulated digestion conditions. Their micro- and nanostructural changes were studied using microscopy, laser diffraction and small angle X-ray scattering. Both the molecular weight and M/G ratio affected the size and nanostructural features of the capsules, but the changes in gastrointestinal conditions were mainly determined by the latter. All microcapsules swelled slightly in simulated gastric fluid (pH=3) and swelled further in simulated intestinal fluid (pH=7), particularly those with high mannuronic acid (M) contents. While high guluronic acid (G) beads maintained the nanostructural features characteristic of alginate gels (junction zones) in both media, these were rapidly disrupted in the M-rich capsules. Decreasing the pH of the gastric phase from 3 to 2 had dramatic structural impacts, resulting in a greater integrity of the microcapsules, thus highlighting the importance of the selected digestion protocol for rational microcapsule design.

KEYWORDS

Alginate, microcapsule, hydrogel, digestion, SAXS, synchrotron

1. Introduction

The development of food-grade microencapsulation strategies for the production of new functional foods has attracted increasing commercial interest from the food industry in the last decades (Ozen, Pons, & Tur, 2012). Edible biopolymers with hydrogel-forming abilities are of particular interest in this area, since their chemical and structural properties promote the formation of polymeric networks capable of protecting sensitive bioactive ingredients entrapped within them (Gómez-Mascaraque, Soler, & Lopez-Rubio, 2016). These bioactive ingredients should be subsequently released from their encapsulation matrices in a controlled manner, ideally at a particular target site (usually the small intestine) (Gómez-Mascaraque, Llavata-Cabrero, Martínez-Sanz, Fabra, & López-Rubio, 2018).

Alginates, natural polysaccharides extracted from the cell walls of brown algae (Rioux & Turgeon, 2015), are one of the most widely used materials for encapsulation (Chan, Lee, Ravindra, & Poncelet, 2009) and are being extensively used as food-grade delivery vehicles due to their ability to gel under mild conditions by ionic crosslinking with divalent cations such as Ca^{2+} (Ramos et al., 2018). Moreover, alginates have been reported to form stronger hydrogel networks under gastric conditions, which become weaker in the intestinal environment (Hoad et al., 2009; Rayment et al., 2009). This behaviour has been attributed to the pH sensitivity of alginates (Chuang et al., 2017) and the scavenging of Ca^{2+} from the gel matrix due to the presence of calcium chelators in the intestinal environment (Strobel, Scher, Nitin, & Jeoh, 2016), and makes them an attractive option as intestinal-targeted delivery vehicles.

The gelling ability and pH sensitivity of alginates is the result of their particular chemical structure. They consist of (1→4)-linked β-D-mannuronic acid (M) and α-L-guluronic acid (G) residues randomly distributed along linear polysaccharide chains (de Celis Alonso et al., 2010), forming MM-blocks (consecutive M residues), GG-blocks (consecutive G residues) and MG-blocks (alternating M and G residues) (Grasdalen, Larsen, & Smisrod, 1981). The G residues of alginates have a greater affinity for Ca^{2+} due to their steric conformation (Ramos et al., 2018), so their gelation behaviour has been attributed mainly to interactions between the Ca^{2+} ions and G residues (Gombotz & Wee, 1998; Strobel et al., 2016), which lead to the crosslinking of the polymeric chains through the formation of junction zones (Schuster, Wallin, Klose, Gold, & Ström, 2017; Smidsrød, 1974). The model generally used to describe these junction zones, and the tridimensional network to which they give rise, is known as the "egg-box" model, in which calcium ions are positioned between consecutive G residues (Grant, Morris, Rees, Smith, & Thom, 1973; Simpson, Stabler, Simpson, Sambanis, & Constantinidis, 2004).

Currently, there is no universal consensus on what characteristics of alginates are more desirable for microencapsulation purposes [6]. On one hand, G-rich alginates are reported to generate more ordered and stiffer hydrogels, which maintain their integrity for longer periods of time (Simpson et al., 2004). However, due to the greater rigidity of G-blocks (Hecht & Srebnik, 2016), these result in gels with larger pores than M-rich alginates [6], which make it easier for the immobilised bioactive ingredients to diffuse out of the polymeric network. In contrast, M-rich alginates have been described as less viscous, and this allows processing of higher alginate concentrations, which together with smaller pores, reduce the diffusion permeability of the capsules produced (Klöck et al., 1997). Capsules prepared with M-rich alginates are softer and tend to disintegrate with time, and are subject to a higher degree of shrinking during crosslinking (Simpson et al., 2004), which can impact negatively on encapsulation efficiency.

The performance of alginate microcapsules prepared from alginates with different characteristics during gastrointestinal digestion also needs to be taken into account when these are intended for food or oral drug applications. However, most of the works on gastrointestinal digestion of alginate capsules have used a single alginate grade only (Chuang et al., 2017; Hoad et al., 2009; Rayment et al., 2009). Ramos et al. (2018) recently reported that capsules made of alginates with higher molecular weights exerted a weaker protective effect on probiotic bacteria during *in vitro* gastrointestinal digestion. This was attributed to the formation of hydrogels with bigger pores that facilitated exposure of the immobilised cells with the harsh gastric conditions (Ramos et al., 2018). The effects of M/G ratio, however, were not discussed.

The aim of the present work was to study and correlate the micro- and nanostructural evolution of alginate microcapsules under simulated digestion conditions, and to relate the impact of the M/G ratio and molecular weight of the alginates used to produce them on the changes observed. For this purpose, three different alginate grades, with different M/G ratios or molecular weights, were used to produce alginate microcapsules by external gelation in $CaCl_2$. The capsules were then incubated in simulated digestive fluids and their micro-and nanostructure, both as-prepared and after incubation, was characterised by means of microscopy, laser diffraction and small angle X-ray scattering techniques.

2. Materials and Methods

2.1. Materials

Three pure (>99%) food grade sodium alginate grades, under the commercial names of Manucol DH (35-40%G, 40-90 mPa·s), Manugel GHB (60-65%G, 50-100 mPa·s) and

Protanal RF6650 (60-65%G, 400-600 mPa·s), and referred to as LowG, HighG and HighG-High$_{Mw}$, respectively, were kindly donated by DuPont Nutrition & Health (Norway). Calcium chloride di-hydrate, 37% hydrochloric acid, sodium hydroxide and all inorganic salts used to prepare the simulated digestive fluids were purchased from Sigma-Aldrich (Ireland).

2.2. Characterization of the sodium alginates

2.2.1. Rheological properties

The viscosity of the sodium alginate aqueous solutions was studied using an AR-2000 (TA Instruments, USA) rheometer with a parallel plate geometry (60 mm diameter and 500 μm gap) following a procedure adapted from (Gómez-Mascaraque, Lagarón, & López-Rubio, 2015). Continuous shear rate ramps were performed from 0.1 to 500 s^{-1} over 10 min at a controlled temperature of 25 ºC, following pre-shear treatment at $1s^{-1}$ for 10 s and equilibration for 1 min. The shear stress of the samples was registered during the experiment. The flow obtained curves were fitted to the Ostwald de Waele model according to Eq. (1), were σ is the shear stress, K the flow consistency index, γ the shear rate, and n the flow behaviour index (Gómez-Mascaraque et al., 2018). All measurements were made at least in triplicate.

$$\sigma = K \cdot \gamma^n \qquad \text{Eq. (1)}$$

2.2.2. High performance size exclusion chromatography (HPLC-SEC)

The molecular weight distribution of the alginates was obtained through HPLC-SEC analyses following the method described in (Martínez-Sanz et al., 2019), using a high performance liquid chromatography system equipped with a Waters 2695 separations module and a Waters 2414 refractive index detector (Waters, USA). The samples (1 mg/mL) were dissolved in the mobile phase (0.05 M Na_2SO_4/0.01 M EDTA, adjusted to pH 7) (Kristiansen, Tomren, & Christensen, 2011) at 40 °C for 1h, filtered through 0.8 µm pore syringe filters for aqueous media (Sartorius, Germany), and injected into an OHpak SB-800 HQ size exclusion chromatography column (Shodex, Japan) equilibrated at 40 °C. The injection volume was 20 µL and the flow rate was 0.5 mL/min. Calibration was performed using P-82 pullulan standards (Shodex, Japan), and peak molecular weights (M_p) are reported.

2.2.3. Raman microspectroscopy

Raman spectra of the alginates were recorded using an Alpha300 R confocal Raman microscope (WITec, Germany) equipped with a 532 nm laser and an ultra-fast Raman imaging CCD camera. A 20× microscope objective was used to collect the spectra at a laser power of 20 mW, with an integration time of 1s and 20 accumulations were averaged. These conditions were chosen to avoid sample degradation. The raw spectra were processed using the Savitzky-Golay smoothing function (order 2, gap size 5) and a shape function (shape size 150, noise factor 1) for background subtraction using the Project Five software v5.0 (WITec, Germany).

2.3. Production of alginate microcapsules

Sodium alginate solutions were prepared by dissolving the polysaccharides in deionized water (0.75% w/v) under intense magnetic agitation overnight, and subsequently filtered through 0.8 μm pore syringe filters for aqueous media (Sartorius, Germany).

Alginate microcapsules were produced using an Inotech Encapsulator IER-50 (Inotech Biosystems Intl. Inc., Switzerland), by extrusion of the alginate solutions through a 200 μm nozzle at a flow rate of 5 mL/min into a gelling bath (140 mm diameter) containing 250 mL of 0.1 M $CaCl_2$. The gelling bath was located at a distance of 16 cm from the nozzle and maintained under constant agitation. Alginate droplet formation and break up was aided by a nozzle vibration frequency of 1460 Hz and an applied voltage of 0.8 kV, as optimized in preliminary trials. The collection time was set at 5 min for each batch, and the microcapsules were cured within the gelling solution for 30 min before being filtered and thoroughly washed with deionized water.

2.4. Morphological characterization of the microbeads

Optical microscopy images were taken using an Olympus BX51 digital microscopy system (Olympus Corporation, Japan) equipped with a ProgRes CT3 digital camera head (Jenoptik, Jena, Germany). ProgRes CapturePro software (v 2.10.0.0) was used for image capturing.

2.5. Particle size distribution

The particle size distribution of the microbeads was determined by laser diffraction using a Malvern Mastersizer 3000 apparatus equipped with a Hydro MV accessory for liquid samples (Malvern Instruments, UK). A refractive index of 1.4683 and an absorption index of 0.01 were used.

2.6. Water content of the microcapsules

The capsules (ca. 2 g) were filtered and accurately weighted before and after freeze-drying in order to estimate their water content, which was calculated according to Eq. (2), where m_h is the mass of the hydrated capsules and m_d is the mass of the dry capsules. Measurements were performed in triplicate.

$$Water(\%) = \frac{m_h - m_d}{m_h} x100 \qquad \text{Eq. (2)}$$

2.7. Small and wide angle X-ray scattering (SAXS)

Small angle X-ray scattering (SAXS) experiments were carried out in the Non Crystalline Diffraction beamline, BL-11, at ALBA synchrotron light source (www.albasynchrotron.es). The energy of the incident photons was 12.4 KeV (an equivalent wavelength, λ, of 1 Å). The SAXS diffraction patterns were collected by means of a single-photon counting detector, Pilatus 1 M, with an active area of 168.7×179.4mm^2, an effective pixel size of 172×172 μm^2 and a dynamic range of 20 bits. The sample-to-detector distance was set to 7740 mm, resulting in a q range with a maximum value of q=0.189 Å^{-1}. An exposure time of 2 s was selected on the basis of preliminary measurements in order to maximize the signal to noise ratio while avoiding detector saturation.

The data reduction was treated by pyFAI python code (ESRF) (Kieffer & Wright, 2013), modified by ALBA beamline staff in order to obtain on-line azimuthal integrations from a previously calibrated file. The calibration files were created from Silver behenate (AgBh). The intensity profiles were then represented as a function of q using the IRENA macro suite (Kieffer & Wright, 2013) within Igor procedures. A scattering background (corresponding to a quartz capillary filled with water, simulated gastric fluid or simulated intestinal fluid, depending on the sample) was subtracted from all the samples. The experimental data were fitted using a function consisting of a two-level Beaucage model. This model considers that, for each individual level, the scattering intensity is the sum of a Guinier term and a power-law function (Beaucage, 1995, 1996).

$$I(q) = \sum_{i=1}^{N} G_i \exp\left(-q^2 \cdot \frac{R_{g,i}^2}{3}\right) + \frac{B_i\left[\operatorname{erf}(qR_{g,i}/\sqrt{6})\right]^{3P_i}}{q^{P_i}} + bkg \qquad \text{Eq. (3)}$$

where $G_i = c_i V_i \Delta SLD_i^{\,2}$ is the exponential prefactor (where V_i is the volume of the particle and ΔSLD_i is the scattering length density (SLD) contrast existing between the ith structural feature and the surrounding solvent), $R_{g,i}$ is the radius of gyration describing the average size of the ith level structural feature, B_i is a q-independent prefactor specific to the type of power-law scattering with power-law exponent, P_i, and bkg is the background.

2.8. Experiments under simulated gastrointestinal conditions

Simulated gastric fluid (SGF) and simulated intestinal fluid (SIF) were prepared according to the compositions described in the INFOGEST standardised method (Brodkorb et al., 2019; Minekus et al., 2014) and adjusted to pH 3 and 7, respectively. The gastric phase of the gastrointestinal digestion was simulated by mixing a suspension of the alginate microcapsules in water (10% w/w) with SGF (50:50 v/v) and incubating it at 37 ºC for 2h. The intestinal phase of the digestion was subsequently simulated by adding SIF (50:50 v/v) to the previous capsule suspensions and incubating them at 37 ºC for 2h. After different time intervals, samples were analysed in terms of size, morphology and nanostructure as described in Sections 2.4, 2.5 and 2.7.

2.9. Impact of the pH on the alginate microcapsules

To assess the influence of the pH of simulated fluids on the size, morphology and nanostructure of the alginate microcapsules, SGF was prepared according to the compositions described in (Brodkorb et al., 2019; Minekus et al., 2014), but was subsequently adjusted to different pHs in the range from 1 to 8. These media were then used to incubate the microcapsules for 2h at 37 ºC as described in Section 2.7.

2.10. Statistical analysis

IBM SPSS Statistics software (v.24) (IBM Corp., USA) was used to perform the statistical analysis of the data. Shapiro-Wilk and Levene tests were performed to confirm the normality of the data and the homogeneity of variances, respectively. The statistical significance of the differences observed between samples was assessed through one-way ANOVA, using the Bonferroni post-hoc test for multiple comparisons. The significance level was fixed at $\alpha = 0.05$ for all tests.

3. Results and discussion

3.1. Characterization of the commercial alginate grades

3.1.1. Rheological properties and molecular weight

Figure 1A shows the rheological profile (flow curves) of alginate solutions prepared with the three different sodium alginate grades used, i.e. LowG, HighG and HighG-High$_{Mw}$, at the concentration used to produce the microcapsules, that is, 0.75% w/v (cf. Section 2.3). The shear stress *vs*. shear rate curves obtained were fitted to the Ostwald de Waele model, and the resulting equations are also presented in Figure 1A. Additionally, Figure 1B shows the viscosity of the alginate solutions at $\gamma = 10\ s^{-1}$ as a function of the polysaccharide concentration. This shear rate was selected for comparison since it is equivalent to that experienced typically by polymer solutions when subjected to extrusion processes under gravity (Chan et al., 2009).

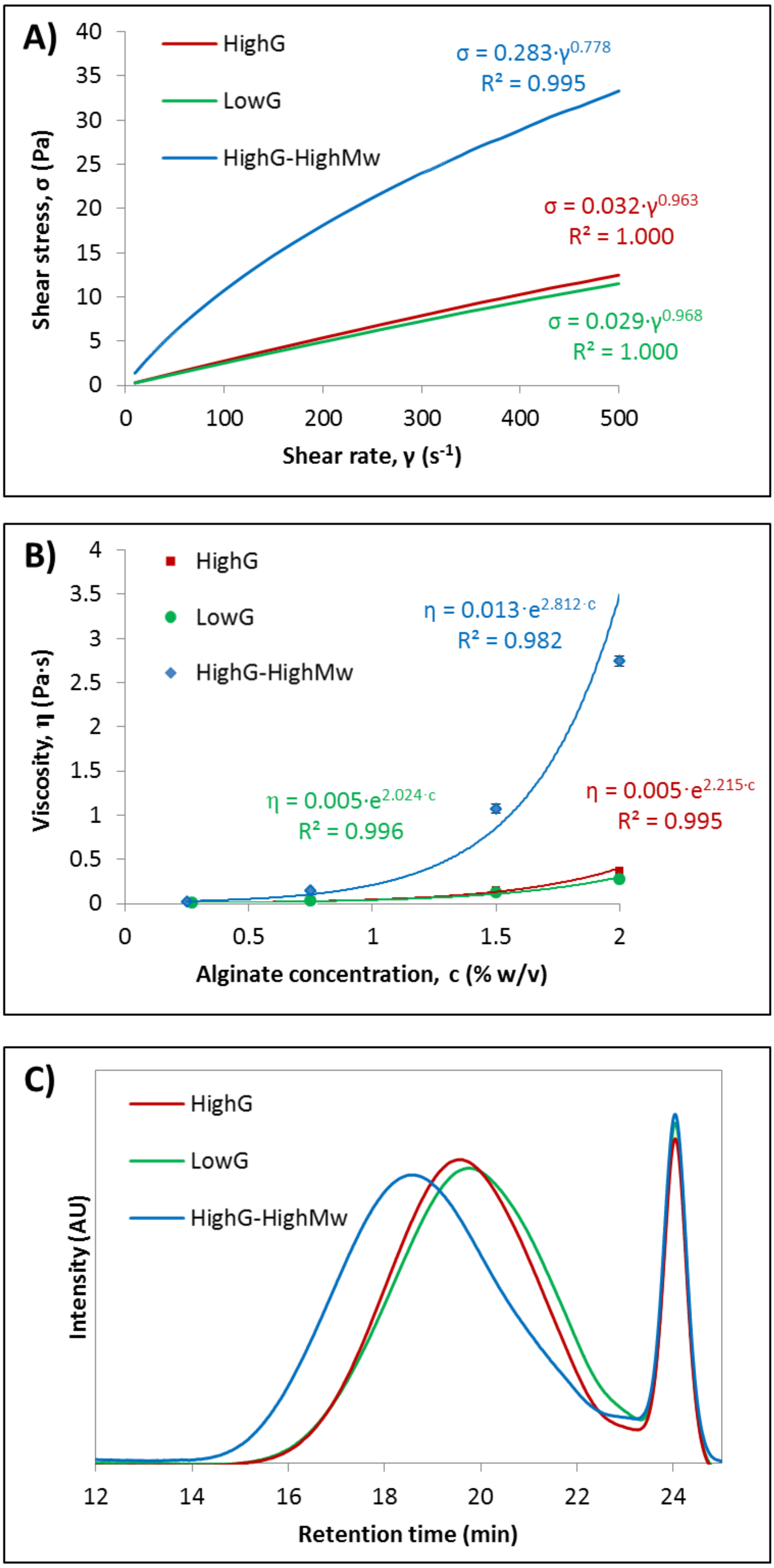

Figure 1. A) Rheological behaviour (shear stress vs. shear rate curves) of alginate solutions (0.75% w/v), fitted to the Ostwald de Waele model. B) Viscosity (at γ=10s^{-1}) of alginate solutions as a function of polymer concentration. C) HPLC-SEC chromatograms of the alginates

The viscosity of the alginate solutions increased exponentially with the polymer concentration, as previously reported for alginates (Chan et al., 2009; Davarcı, Turan, Ozcelik, & Poncelet, 2017), and the results were consistent with the viscosity values provided by the supplier. Indeed, the viscosity of LowG and HighG was very similar, and significantly lower than that of HighG-High$_{Mw}$. Moreover, the flow behaviour of the former two was very similar and close to that of Newtonian fluids at 0.75% w/v concentration, as inferred from their flow behaviour indexes which were very close to 1 (0.968 and 0.963, respectively). On the contrary, HighG-High$_{Mw}$ showed a shear thinning (pseudoplastic) behaviour at the same concentration, with a lower flow behaviour index (0.778) and a higher flow consistency index (one order of magnitude higher than for the other two). These results suggested that the molecular weight of LowG and HighG was very similar, and considerably lower than that of HighG-High$_{Mw}$.

In order to confirm this, the molecular weight distribution of the three alginate grades was estimated using HPLC-SEC. The chromatograms obtained, shown in Figure 1C, presented a narrow band at a retention time of 24 min corresponding to the void volume of the column (Martínez-Sanz et al., 2019), and a broader band at lower retention times ascribed to the elution of the alginates. The HPLC-SEC analysis confirmed that the molecular weight distributions of HighG and LowG were indeed very similar. The molecular weight of each alginate grade was estimated by extrapolation from a calibration curve built using pullulan standards (R^2 = 0.991), and were lower for HighG and LowG (582 ± 18 and 516 ± 1 kDa, respectively), than for HighG-High$_{Mw}$ (1640 ± 38 kDa).

Therefore, it was considered reasonable that the differences observed between capsules prepared with HighG and LowG were attributable mainly to their different M/G ratios (cf. Section 3.1.2), whereas the differences between those prepared with HighG and HighG-High$_{Mw}$ were mostly due to their different molecular weight.

3.1.2. Raman microspectroscopy

Figure 2 shows the Raman spectra of the different sodium alginate grades. The three spectra showed the characteristic bands of alginate, which have been intensively described and assigned elsewhere (Campos-Vallette et al., 2010; Hernández, Sacristán, & Mijangos, 2010; Salomonsen, Jensen, Stenbæk, & Engelsen, 2008). The relative intensity of certain bands in the Raman spectra of alginates has been reported to vary according to the M/G ratio and their sequence of homopolymeric (GG, MM) and heteropolymeric (GM) blocks (Campos-Vallette et al., 2010). According to Salomonsen et al. (2008), the bands most sensitive to differences in M/G ratios are that centred at about 806 rel. cm^{-1}, whose relative intensity increases with decreasing M/G ratios, and that centred at about 955 rel. cm^{-1}, whose relative intensity increases with increasing M/G ratios. The relative intensities of those bands varied in the following order: HighG > HighG-High$_{Mw}$ > LowG for the band centred at 808-810 rel. cm^{-1}, and HighG < HighG-High$_{Mw}$ < LowG for the band centred at 956 rel. cm^{-1}. Although differences in the sequence of GG, MM and GM blocks along the polymeric chain may also have an impact on the Raman spectra of the sample, these results confirmed that the M/G ratio of LowG was indeed higher than that of HighG and HighG-High$_{Mw}$, as indicated by the supplier.

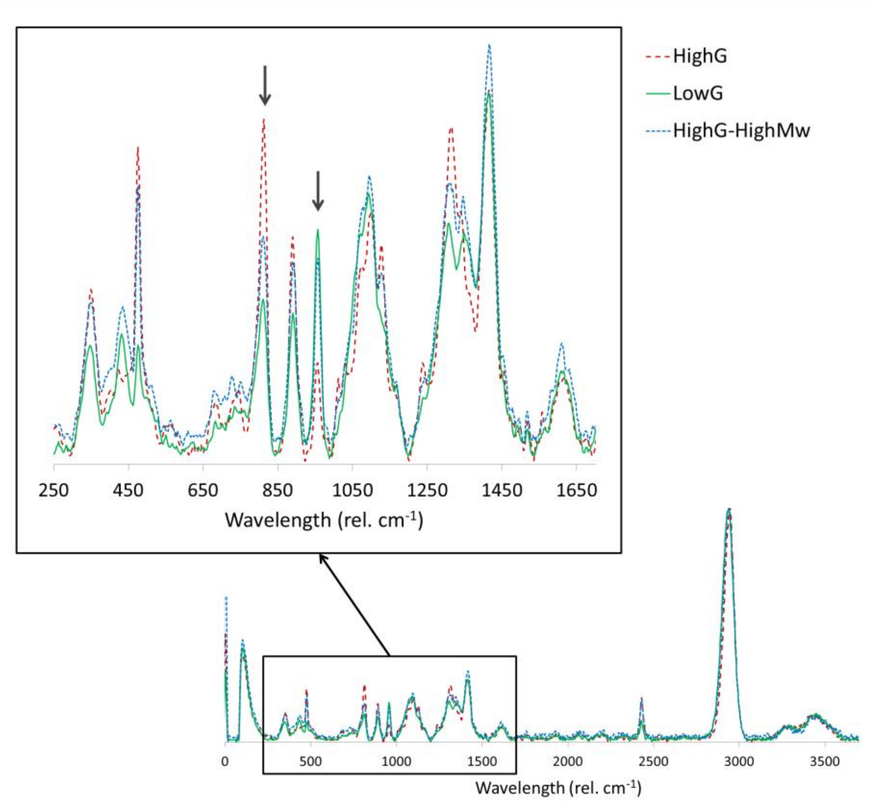

Figure 2. Normalized Raman spectra of the different alginate grades obtained by Raman microspectroscopy

3.2. Impact of the M/G ratio and molecular weight on alginate microbeads

3.2.1. Size and morphology

Alginate microcapsules were produced through the extrusion-external gelation method using three different alginate grades under the same processing conditions (cf. Section 2.3). 0.75% (w/v) was the maximum concentration that could be processed using HighG-High$_{Mw}$, the most viscous of the alginates examined, and so this concentration was selected for microcapsule production using the three alginates. Figure 3 shows representative micrographs of the microbeads, and their particle size distributions, measured by laser diffraction, are depicted in Figure 4A.

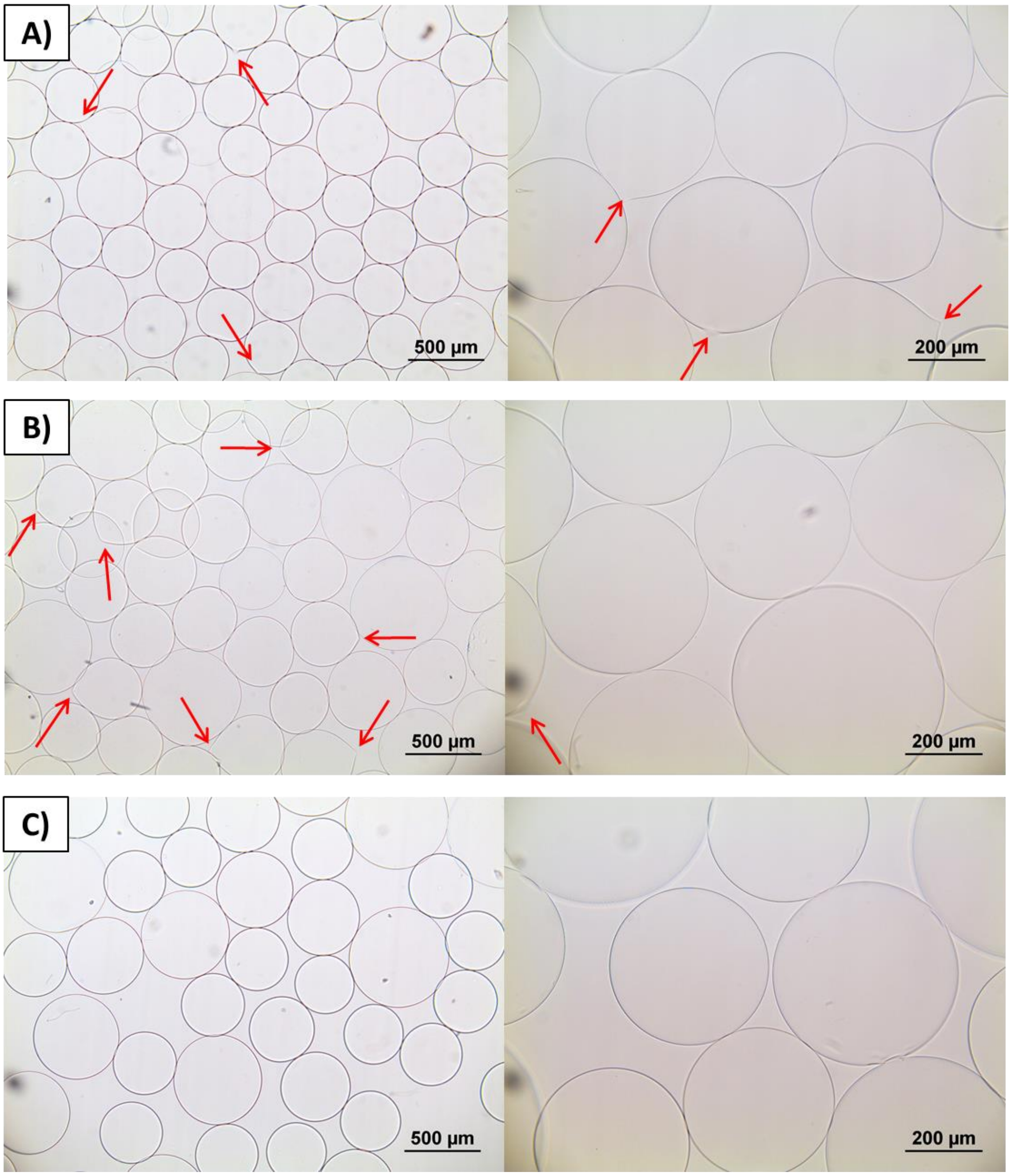

Figure 3. Micrographs of alginate microbeads produced using HighG (A), LowG (B) and RF6650HighG-High$_{Mw}$ (C) alginate grades. Arrows in the images indicate bead defects.

The smallest microbeads (average size D [4,3] = 380±2 μm) were obtained using the alginate with the lowest molecular weight and highest guluronic acid content (i.e. HighG). These also exhibited the narrowest size distribution. An increase in the M/G ratio (i.e. LowG) or an increase in the molecular weight (HighG-High$_{Mw}$) resulted in bigger and more polydisperse microbeads (D [4,3] = 466±5μm and 444±2 μm for LowG and HighG-High$_{Mw}$ microbeads, respectively). Indeed, alginates with higher molecular weights exhibit greater viscosities (cf. Section 3.1.1), which result in greater droplet sizes and, thus, bigger capsules, when using vibrating nozzle technologies for bead production under the same disturbance frequency (Del Gaudio, Colombo, Colombo, Russo, & Sonvico, 2005).

On the other hand, the M/G ratio has also been reported to have an impact on the size of alginate microbeads, since it affects the shrinkage, also known as syneresis, that the alginate droplets experience upon crosslinking to form microhydrogels, (Chan et al., 2009). Previous works reported that lower M/G ratios led to less shrinkage than high M/G ratios, resulting in larger microcapsules (Chan et al., 2009; Kendall, Darrabie, El-Shewy, & Opara, 2004; Ramos et al., 2018). This could be due to the greater flexibility and, thus, greater shrinking capability, of the polymeric chains of alginates with higher M/G ratios, since the stiffness and relative unperturbed dimensions of alginate blocks are known to increase in the order: MG-blocks < MM-blocks < GG-blocks (Hecht & Srebnik, 2016; Smidsrød, 1974). However, the opposite trend was observed in this work. This could be explained taking into account that capsules were washed thoroughly with deionized water to remove excess of calcium chloride prior to analysis, whilst this step was not reported in the aforementioned works. Upon washing with deionized water, calcium alginate capsules are expected to swell due to an osmotic effect (Davarcı et al., 2017), and since lower M/G ratios lead to higher crosslinking of the alginate hydrogel networks, lower swelling capacities would be expected for alginates with high G contents.

To confirm this hypothesis, micrographs of HighG and LowG capsules in 0.1M $CaCl_2$ (before washing) were also taken (cf. Figure S1 of the Supplementary Material). While both types of microbeads swelled upon washing, this swelling was notably more pronounced in those with the highest M/G ratios, which were initially smaller but became larger after washing. The water content of the washed microcapsules was also determined as described in Section 2.6. Indeed, the water content of the beads prepared with LowG (99.26 ± 0.08 %) was significantly higher (cf. Figure S2 of the Supplementary Material) than that of HighG (98.99 ± 0.04 %) and HighG-High$_{Mw}$ (98.92 ± 0.06 %), despite having been prepared from the same alginate concentration, which suggests that the swelling capacity of the hydrogel network of the former was greater. These findings highlight the need to assess the particle size distribution of alginate microcapsules, in the medium of interest for their intended application, rather than just as-prepared.

Figure 3 also shows the presence of defects in some of the alginate microcapsules (highlighted with arrows), particularly in those produced from lower molecular weight alginates (i.e HighG and LowG). These defects have been previously reported for capsules produced from low viscosity alginate solutions and are attributed to a droplet shape deformation upon impact with the gelling bath when viscous and surface tension forces of the alginate solution are too low to overcome the effect of impact and drag forces in the gelling bath (Chan et al., 2009; Davarcı et al., 2017). In practice, these deformations can be avoided by increasing the alginate concentration and, as a result, the viscosity of the solutions. However, for the purpose of this work, all alginate solutions were prepared at the same concentration to allow direct comparison, resulting in some being more viscous than others.

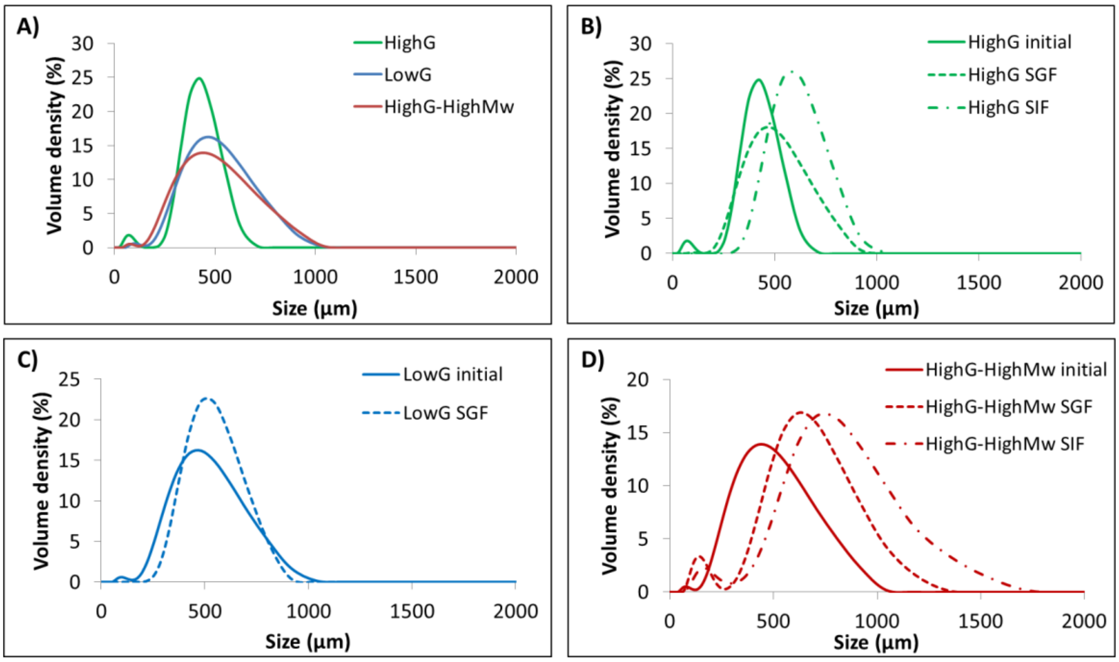

Figure 4. Size distribution of alginate microbeads produced using three alginate grades (A). Microbeads prepared from HighG (B), LowG (C) and HighG-High$_{Mw}$ (D) after incubation in simulated digestive fluids. SGF and SIF stand for simulated gastric and intestinal fluids, respectively.

3.2.2. Nanostructural features

To investigate the influence of M/G ratio and molecular weight on the nanostructure of alginate microbeads, SAXS experiments were carried out. Figure 5A shows the scattering patterns obtained, as well as the theoretical fitting curves obtained using the mathematical model described in Section 2.7. The scattering patterns, characterized by the appearance of a shoulder-like feature and a power-law region at lower q values, were similar to those reported previously for calcium alginate gels (Agulhon, Robitzer, David, & Quignard, 2011; Draget, Skjåk-Bræk, & Stokke, 2006). The presence of scattering features in calcium-alginate gels has been ascribed to the existence of junction zones arising from the association of alginate chains, driven by the presence of calcium cations, as described by the egg-box model (Draget et al., 2006; Grant et al., 1973). The estimated fitting parameters (cf. Table S1), suggested structural differences between the three types of alginates. Whereas a power-law exponent (P_1) of 1.6, indicative of fractal structures with a polymeric chain arrangement similar to that of swollen chains, was calculated for the HighG-High$_{Mw}$ microbeads, the LowG and HighG microbeads had power-law exponents of 1.9 and 2.3, respectively, which are consistent with the presence of more aggregated or entangled fractal-like structures. A second power-law exponent (P_2) of 4.0 was obtained to account for the higher q region ($q>0.1Å^{-1}$) in the three samples, indicating the existence of sharp interfaces. The associated radii of gyration (R_{g2}), which can be related to the size of the junction zones, was 4.1 nm for HighG-High$_{Mw}$, 5.7 nm for LowG and 6.0 nm for HighG microbeads. These results suggest the existence of more densely packed and ordered structures in the case of the higher molecular weight alginate HighG-High$_{Mw}$, whereas alginate chains seemed to be associated in a less ordered fashion in the case of HighG and LowG, as illustrated in the schemes proposed in Figure 5B. To the best of our knowledge, the effect of the molecular weight on the association of alginate chains has not been studied extensively, but it seems that the greater viscosity of HighG-High$_{Mw}$ solutions gave rise to tighter molecular chain packing. Although the M/G ratio did not seem to affect the size of the junction zones, it had a significant impact on the physical density of the gel structures formed. This is deduced from the lower scattering intensity of the LowG microbeads at $q > 0.02Å^{-1}$. Since the scattering intensity is directly proportional to the scattering length density (SLD) contrast (in this case, the SLD difference between the alginate gel and the surrounding water), the lower intensity in the case of the LowG sample suggests a less dense gel network, i.e. a greater hydration level. Indeed, previous work has demonstrated that aggregates formed as a result of alginate-Ca^{+2} interactions are stiffer in molecular chain segments richer in G (Hecht & Srebnik, 2016), making the gel network less accessible to water. The higher water content of LowG microbeads does not affect the size of the alginate-calcium junction zones, but it is expected to affect the arrangement of the chain aggregates, forming a more swollen gel network structure. The appearance of scattering features characteristic of this gel network structure seems to be out of the range covered by the SAXS experiments.

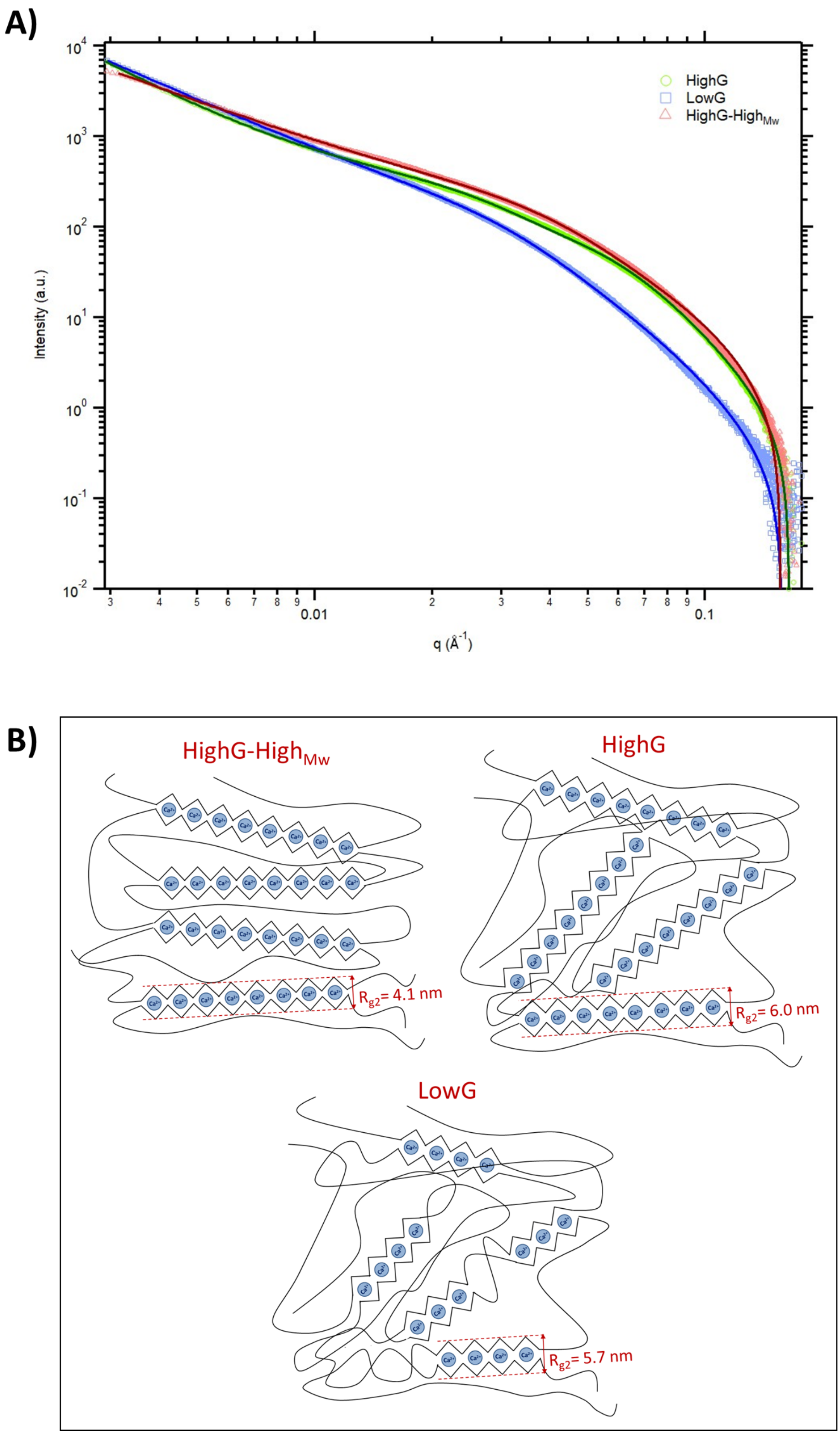

Figure 5. A) SAXS patterns from alginate microbeads. Solid lines represent the theoretical fitting curves obtained using a two-level Beaucage function. B) Scheme illustrating nanostructural differences among the microhydrogels prepared with the different alginates: HighG-High$_{Mw}$ exhibited lower R_{g2} and a more densely packed and ordered structure than LowG and HighG. LowG shows less amount of G residues.

3.3. Impact of *in vitro* gastrointestinal digestion on the alginate microbeads

In order to assess the micro- and nanostructural changes undergone by the alginate microcapsules upon digestion, these were subjected to simulated gastrointestinal conditions, as described in the standardised static *in vitro* digestion method, developed within the INFOGEST international network (Brodkorb et al., 2019; Minekus et al., 2014). Accordingly, the microcapsules were incubated in simulated gastric fluid (SGF) at a constant pH of 3, and simulated intestinal fluid (SIF, pH = 7), consecutively, at 37 ºC for 2 h periods. However, no digestive enzymes or bile were added in this study, since their presence could give rise to the appearance of scattering features, interfering with the signal from the alginates and making the interpretation of the SAXS patterns too complex. Since alginates are dietary fibres (Houghton et al., 2015; Wilcox, Brownlee, Richardson, Dettmar, & Pearson, 2014), i.e. non-digestible carbohydrates (Qi & Tester, 2019), this approximation was considered an acceptable approach to study the structural changes in the alginate capsules under simulated gastrointestinal conditions.

3.3.1. Microstructural changes

Figure 6 shows micrographs of beads prepared from HighG, LowG and HighG-High$_{Mw}$, respectively, after 2 h incubation in SGF and after 2 h additional incubation in SIF. Their corresponding size distributions, measured by laser diffraction, are shown in Figure 4B-C.

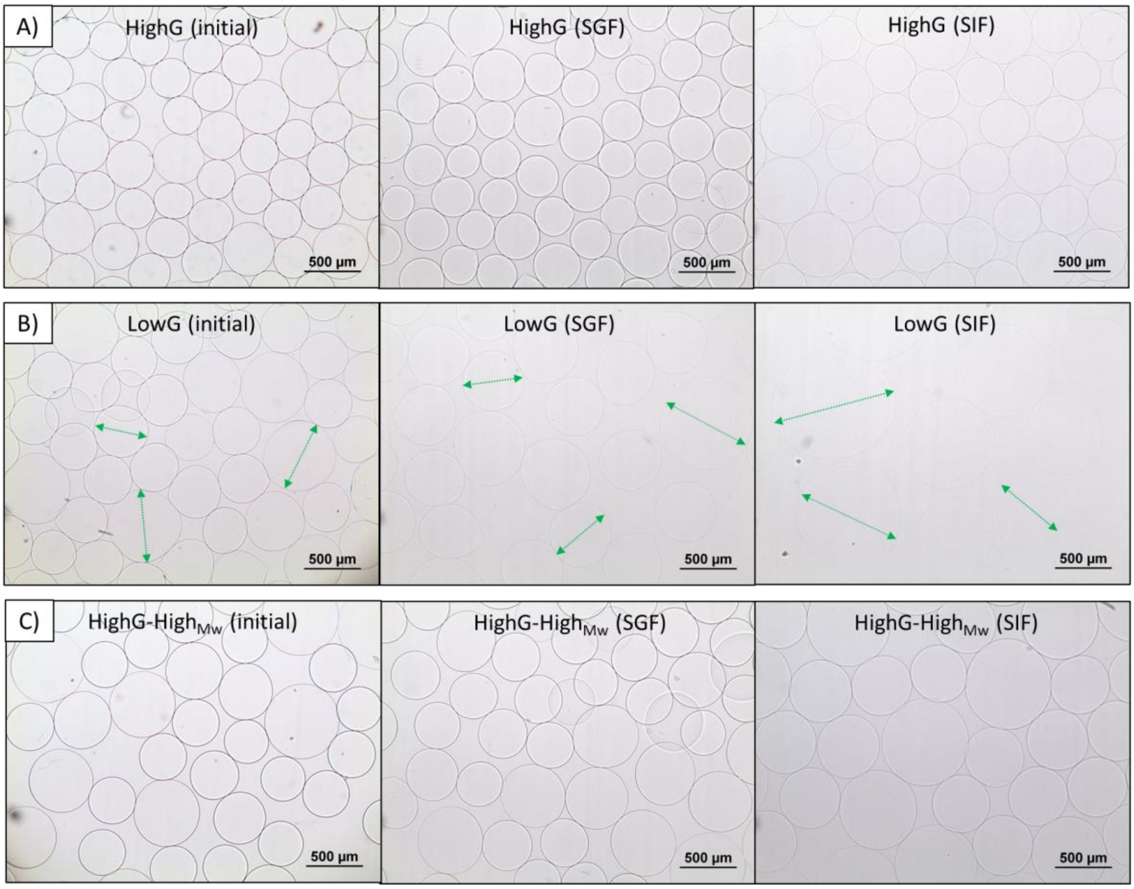

Figure 6. Micrographs of alginate microbeads produced from HighG (A), LowG (B) and HighG-High$_{Mw}$ (C) before and after incubation in simulated digestive fluids. SGF and SIF stand for simulated gastric and intestinal fluids, respectively. Arrows in (B) indicate capsule diameters for some of the beads to facilitate visualization.

According to the results shown in Figure 4, the size of the alginate microcapsules increased slightly following the gastric phase, and increased further following the intestinal phase. Although this increase was not as evident in the micrographs (cf. Figure 6) for the gastric phase, since the changes were more subtle, it was apparent for the intestinal phase. It is widely accepted that alginate capsules swell in intestinal conditions due to an increase in the pH. However, previous works equally report that these shrink in gastric conditions due to the acidic pH found in the stomach, which causes the protonation of free carboxylic groups and, thus, decrease the repulsive charge between alginate chains, allowing them to interact and establish hydrogen bonds (Rayment et al., 2009). This has been generally regarded as one of the main advantages of alginate as a encapsulation matrix, as the potential bioactive agents incorporated within the capsules would be protected during the gastric phase, and would be preferentially released in the intestine (Agüero, Zaldivar-Silva, Pena, & Dias, 2017). Interestingly, the alginate microbeads prepared in this work did not shrink after 2 h incubation in SGF. It was hypothesized that this behaviour could be attributed to the higher pH of the SGF used in the present work (pH = 3) as compared to that employed in other digestion protocols to assess the fate of alginate capsules upon gastrointestinal digestion (i.e. pH=2) (Rayment et al., 2009). To confirm this hypothesis, the pH of the SGF was adjusted to different values and used to incubate the alginate capsules (see Section 3.4).

The pH conditions in static *in vitro* digestion methods can vary considerably depending on the purpose and desired endpoint of the digestion study. A pH of 3.0 in the INFOGEST method (Brodkorb et al., 2019; Minekus et al., 2014), which is a standardised static method for the simulation of food digestion, was justified as an average pH during the dynamic decrease in the digestion of a typical meal in the stomach. Other standardised static methods are used for drug release (Griffin et al., 2014), assess the bioaccessibility of contaminants (Oomen et al., 2003) or mycotoxins from food (Versantvoort, Oomen, Van de Kamp, Rompelberg, & Sips, 2005), with more extreme pHs ranging from 1.2 to 3.

Nevertheless, the pH of the SGF used in this study was lower than the pKa of mannuronic (3.38) and guluronic acid (3.65) residues (Chuang et al., 2017), so the slight increase in the capsules size in this medium appears to have been triggered by factors other than the pH, most probably a high concentration of monovalent cations in the simulated fluids. The weakening of alginate hydrogels in the presence of Na^+ cations has been previously reported and attributed to the competition of these Na^+ ions for the binding sites occupied by Ca^{2+} (LeRoux, Guilak, & Setton, 1999). The concentrations of cations in the simulated fluids were as follows: 7.8 mM K^+, 72.2 mM Na^+, 1 mM NH_4^+, 0.1 mM Mg^{2+} and 0.15 mM Ca^{2+} for the SGF, and 7.6 mM K^+, 123.4 mM Na^+, 0.33 mM Mg^{2+} and 0.6 mM Ca^{2+} for the SIF (Brodkorb et al., 2019; Minekus et al., 2014). In both cases, the concentration of monovalent cations was much higher than that of divalent cations. As a result, part of the Ca^{2+} ion moieties must have been displaced by the monovalent cations present, which explains, at least in part, the weakening of the hydrogel network and the subsequent swelling of the microcapsules. The scavenging of Ca^{2+} had been previously proposed as a mechanism for the weakening of alginate microhydrogel networks in the intestinal environment (Strobel et al., 2016). However, our results showed that this phenomenon also has relevance to the gastric environment.

Regarding the different alginate grades, LowG capsules exhibited the greatest microstructural changes upon incubation in the digestive fluids, looking somewhat more swollen than the rest. In fact, they could barely be observed in the micrographs, as their refractive index became very similar to that of the surrounding simulated digestive fluids (cf. Figure 6B), and they could not be detected properly by laser diffraction following incubation in SIF (cf. Figure 6C). The higher M/G ratio of LowG would also explain its greater sensitivity to both pH and electrolyte changes, due to its lower affinity and selectivity for Ca^{2+} cations (Smidsrød, 1974) and therefore, its greater susceptibility for them to be protonated or displaced by monovalent cations.

3.3.2. Nanostructural changes

SAXS patterns of the alginate microbeads were collected at different time intervals after incubation in simulated gastric and intestinal fluids (Figures 7A, B and C). As observed, in the case of the HighG and HighG-High$_{Mw}$ samples, the shape of the scattering patterns was almost unaffected by simulated digestion. The scattering intensity was seen to decrease slightly after the first 30 min of gastric digestion, remained almost constant throughout the 2h of gastric digestion and then decreased slightly again after the first 30 min of the intestinal digestion. These results suggest that rapid swelling of the microbeads occurred in the simulated digestion fluids, which is in agreement with the increase in their size observed at the microscopic level. However, the amount of fluid penetrating the microbeads must have been small and the gel structure was preserved even after 2 h of intestinal digestion.

On the contrary, an abrupt change in the scattering patterns from the LowG microbeads occurred following 30 min incubation under gastric conditions. The scattering intensity decreased markedly, as observed by the loss of the shoulder-like feature observed in the non-digested sample. Instead, a power-law behaviour characterized by an exponent of ca. -1.7, characteristic from swollen polymeric chains, dominated most of the q range covered by the experiments. The scattering intensity continued to decrease after the first 30 min of incubation in each fluid for LowG beads, as opposed to the faster stabilization of the gels made from high-G alginates. This, together with the micrographs shown in Figure 6, provides evidence for the formation of a highly swollen structure after incubating the LowG microbeads in the simulated digestive fluids. This confirms the essential role of guluronic acid residues in the formation of strong alginate-calcium interactions.

In agreement with the microstructural analysis, the conditions selected for simulating the gastric environment did not result in the strengthening or shrinking of the gel network at the nanostructural level for any of the alginates, as the scattering patterns showed only more extensively swollen structures and, in the case of LowG, even the loss of defined nanostructural features early in the gastric phase.

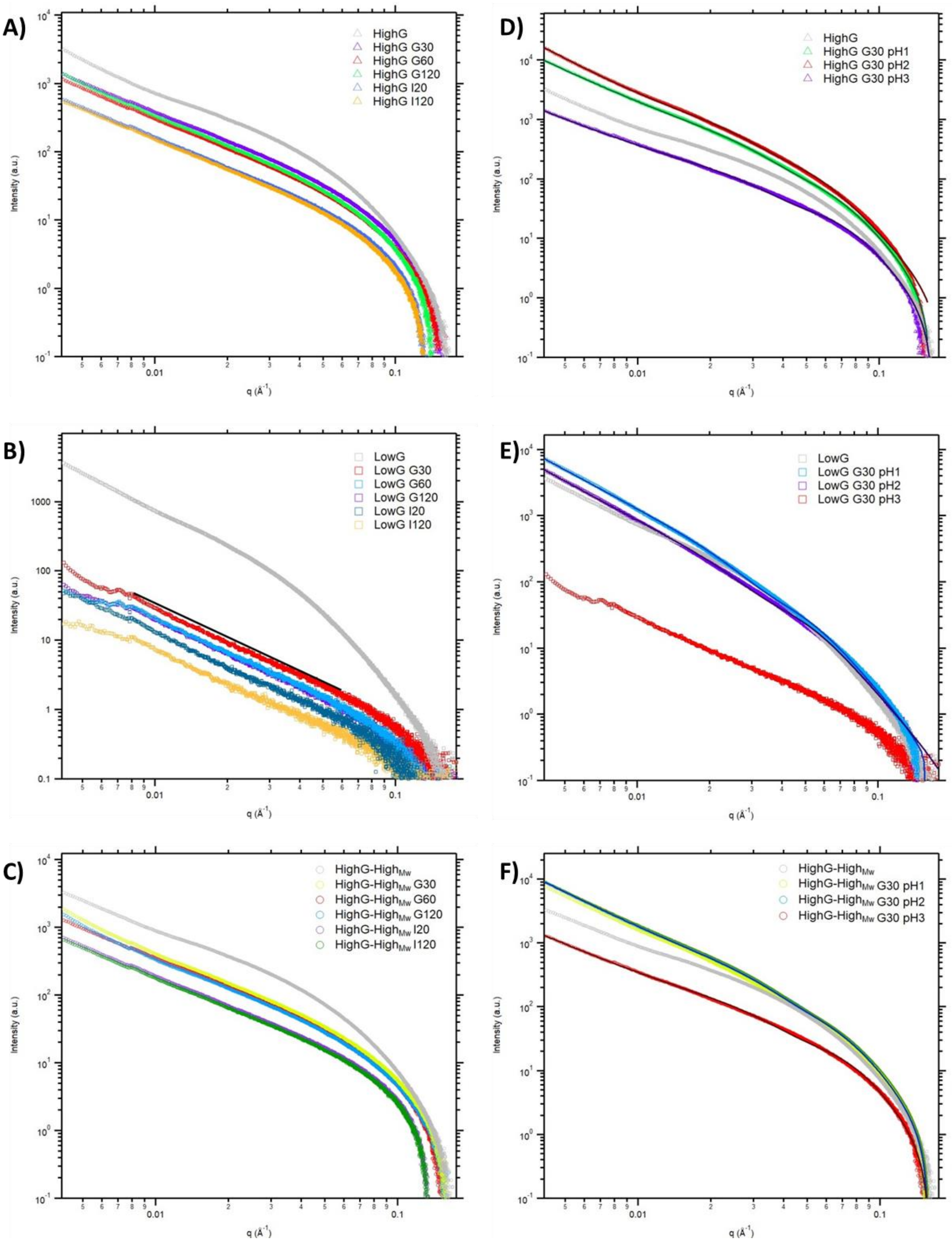

Figure 7. SAXS patterns from alginate microbeads before and after incubation in SGF at pH=3 and SIF at pH=7 for different time intervals (A, B and C). SAXS patterns from alginate microbeads before and after 30 min incubation in SGF adjusted to different pH values (D, E and F). SGF and SIF stand for simulated gastric and intestinal fluids, respectively. Solid lines in D, E and F represent the theoretical fitting curves obtained using a two-level Beaucage function.

3.4. Impact of pH of the SGF on the alginate microbeads

To assess whether the absence of shrinkage of microcapsules in the gastric phase was due to the pH of SGFs used in the present work, SGF was adjusted to different pHs between 1 and 8 before incubating the microbeads. Although the gastric pH applied in the different *in vitro* digestion models found in the literature usually varies between pH 2 and 4 (Brodkorb et al., 2019; Minekus et al., 2014), a wider range was studied in this work to better understand the impact of the pH on the structure of the alginate capsules while keeping the ratio between electrolytes constant.

3.4.1. Microstructural changes

Figure 8 shows the size distribution of the microbeads prepared from the three different alginate grades after 2 h incubation in SGF at different pHs. Figure 9 shows micrographs of the HighG beads after incubation in SGF at selected pHs, as a representative example. The micrographs of the beads prepared using LowG and HighG-High$_{Mw}$ can be found in the Supplementary Material (c.f. Figures S3 and S4).

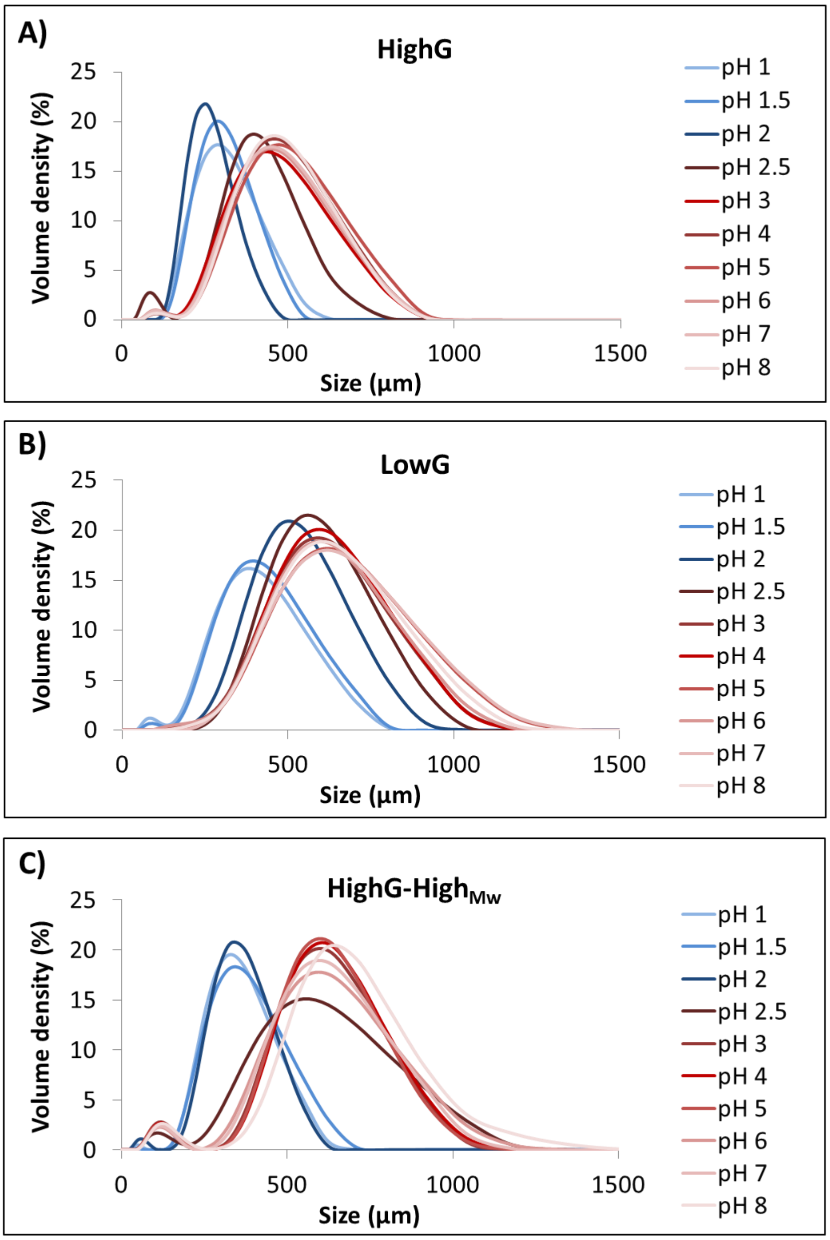

Figure 8. Size distribution of alginate microbeads produced using HighG (A), LowG (B) and HighG-High$_{Mw}$ (C) after 2h incubation in simulated gastric fluids at different pHs.

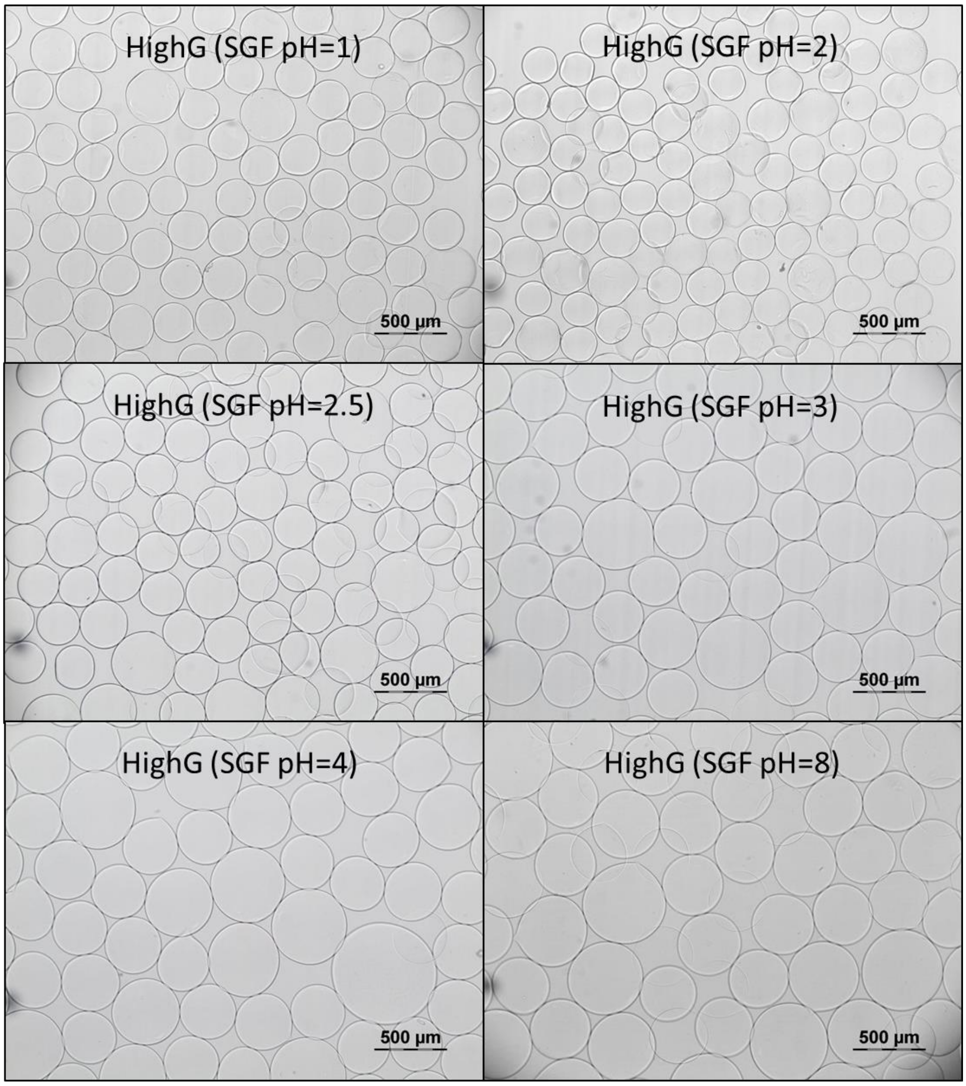

Figure 9. Micrographs of alginate microbeads produced from HighG after 2 h incubation in simulated gastric fluid adjusted at selected pHs.

The results clearly showed the pH-sensitivity of the alginate microbeads, which exhibited larger sizes at higher pH. Figure S5 of the Supplementary Material shows the variation of the median values from the size distributions shown in Figure 8 as a function of the pH, as well as the values for the non-digested samples, to facilitate comparison of the results. In general, the greatest changes in size were observed in the pH range of 1.5 to 3, which is close to the range in which the gastric phase of different digestion protocols tends to differ (Brodkorb et al., 2019; Minekus et al., 2014). This confirms that the different behaviour for alginate capsules observed in the gastric phase in this work, compared to previous studies, can be attributed mostly to the pH of the SGF. This emphasizes the impact that the selected digestion protocol has on the results and conclusions of published work on food digestion. More importantly, the pH in the stomach differs between individuals and is dynamic, i.e. increases to pH 5-7 with meal intake and then gradually decreases to pH 1-2 (Mulet-Cabero, Mackie, Wilde, Fenelon, & Brodkorb, 2019; Mulet-Cabero, Rigby, Brodkorb, & Mackie, 2017; Shani-Levi et al., 2017). Therefore, this work highlights the importance of contrasting the results obtained using static *in-vitro* digestion protocols with assays using dynamic protocols.

In all cases, the microbeads incubated in SGF at pH = 3 exhibited larger capsule sizes than the non-digested samples, while those incubated at pH = 1.5 were smaller. However, the change in size was found to be more gradual for LowG, i.e. the alginate grade with the highest M/G ratio, than for the other two. Also, while for HighG and HighG-High$_{Mw}$, i.e. the G-rich alginates, a pH of 2 was low enough to cause shrinkage of the microcapsules, for LowG the pH had to be lowered further to at least 1.5 to observe a reduction in size with respect to the non-digested samples. LowG has fewer G residues than the other alginates, and was expected to crosslink to a lower extent with Ca^{2+} and, thus, to have a greater amount of free carboxylic groups subject to protonation/deprotonation as a function of pH. As a result, greater pH changes were required to observe size changes for these capsules. This suggested that capsules produced from alginates with high M/G ratios may be more appropriate for applications in which more gradual microstructural changes with pH are pursued.

3.4.2. Nanostructural changes

SAXS experiments were also carried out to characterize the nanostructure of the microbeads after incubation in the simulated gastric fluid adjusted at selected pH values. The pH range between 1 and 3 was selected for this analysis as the major microstructural changes were found to take place within this range. An incubation time of 30 min was selected since it was previously observed that major structural changes occurred within this time frame (cf. Section 3.3.2). The results, shown in Figures 7D, E and F, demonstrated that the pH of the simulated gastric fluid had a strong impact on the structural change observed in simulated digestion conditions. As deduced from the SAXS patterns, the scattering intensity of the samples incubated at pH=1 and pH=2 was higher (HighG and HighG-High$_{Mw}$) or very similar (LowG) to that of non-digested microbeads. This suggests that in this pH range, denser gel structures were formed in the case of the HighG and HighG-High$_{Mw}$ alginates, whereas the density of LowG microbeads was almost unaffected. It would appear that more extensive intra- and intermolecular interactions must have been established due to the protonation of free carboxylic groups and subsequent hydrogen bond formation. At pH 1 and 2, this seemed to be able to counteract the weakening of the LowG gel nanostructure caused by the presence of high concentrations of monovalent ions. For HighG and HighG-High$_{Mw}$, whose nanostructure was less affected by the presence of monovalent cations, these new hydrogen bonds were even able to increase the density of the hydrogel networks. When the pH of the SGF was raised to 3, which is only marginally below the pKa of uronic acid residues (3.38 - 3.65) (Chuang et al., 2017), the scattering intensity of all samples decreased. This effect was much more obvious in the case of LowG due to the existence of weaker alginate-calcium associations, as previously discussed. Hence, at pH 3, the network weakening effect of monovalent cations was found to act predominantly over the strengthening effect of pH.

The fitting results (cf. Table S2) suggested that, at the molecular level, the calcium-mediated association of alginate chains was hardly affected following 30 min gastric digestion for HighG and HighG-High$_{Mw}$ alginates, regardless of the pH of the medium. In the case of the LowG microbeads, the size of the junction zones increased slightly from ca. 5.7 nm for the non-digested samples to ca. 7.2 and 7.1 nm after 30 min incubation in the SGF adjusted to pH=1 and pH=2. Since the affinity of G residues for Ca^{2+} is higher than that of M residues, it is reasonable to expect lower amounts of Ca^{2+} ions interacting with the polysaccharide chains and holding the hydrogel network together in M-rich alginate gels (cf. Figure 5B). Hence, it is also reasonable to presume that, in conditions in which some of the Ca^{2+} ions are replaced by monovalent cations, the interactions holding the junction zones together would become weakened in M-rich alginates such as LowG. The scheme presented in Figure 10 aims to illustrate this phenomenon graphically.

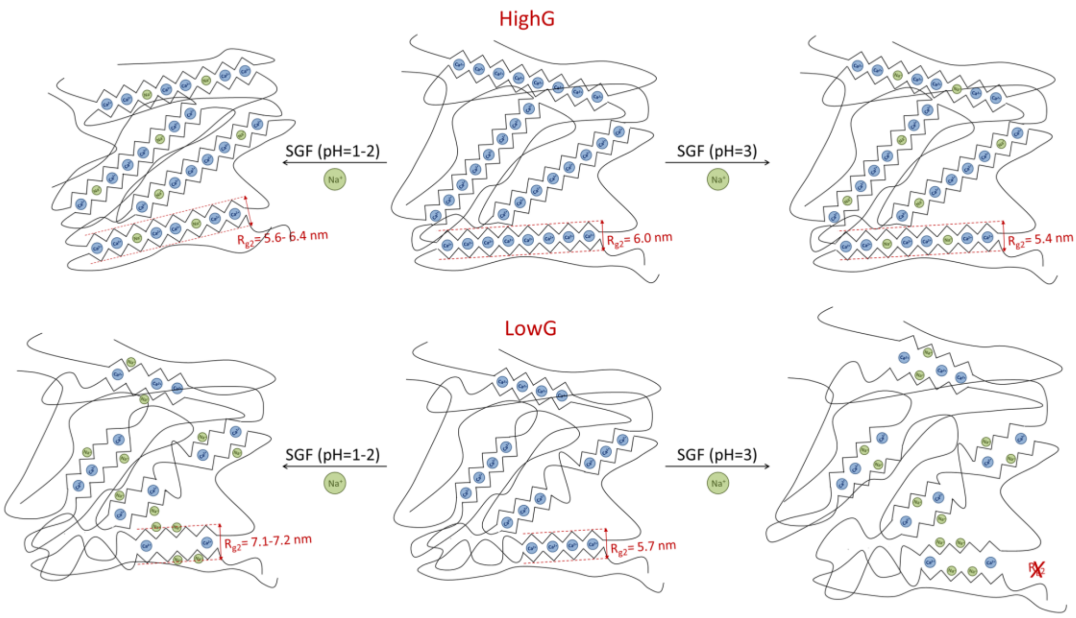

Figure 10. Scheme illustrating nanostructural changes of alginate microhydrogels made from HighG and LowG upon incubation in simulated gastric fluid at different pHs. HighG structures got denser at pH ≤ 2 despite the displacement of Ca^{2+} ions by Na^{+}, whereas the size of the junction zones increased for LowG. At pH = 3, while HighG still maintained the integrity of its junction zones, these were not detected in LowG.

4. Conclusions

The results from this work showed that an increase in either the molecular weight or the M/G ratio of alginates resulted in an increase in the size of the microbeads (once washed with deionised water), due to an increase in the viscosity of the solutions or the swelling capacity of the hydrogel networks, respectively. At the nanostructural level, the alginate with the highest molecular weight gave rise to more densely packed and ordered features, with smaller junction zones, whereas M/G ratio had a greater effect on the density of the hydrogel networks, which was lower for the high-M alginate.

Under simulated gastrointestinal conditions, M/G ratio was the main factor determining the micro- and nanostructural changes of microbeads. The size of alginate capsules increased slightly following incubation in SGF (pH=3) and further increased following incubation in SIF (pH=7), especially for the M-rich alginate. This swelling was consistent with a decrease in the SAXS scattering intensity of the materials following exposure to gastric and intestinal phases, respectively, and was attributed mainly to weakening of the hydrogel networks due to presence of high concentrations of monovalent cations in the fluids. Nevertheless, the junction zones of the G-rich alginates, were not altered significantly by simulated digestion, although they were disrupted to a great extent for M-rich alginate beads after only 30 min incubation in SGF at pH=3.

While it is widely accepted that alginate capsules swell under intestinal conditions, previous works have reported that they shrink under gastric conditions, which is contrary to our findings. By incubating the microcapsules in SGF adjusted to different pHs it was confirmed that these discrepancies were due to the different pH conditions of the gastric phase in the various static digestion protocols reported in the literature. This work highlights the importance of the experimental conditions of the static digestion methods on the conclusions drawn from research work on food digestion, and specifically those involving encapsulation in alginate matrices.

The effect of the pH of SGF was therefore also investigated. The network density of the G-rich gels increased at pH ≤ 2, which was attributed to the formation of more extensive intra- and intermolecular interactions through hydrogen bonding. These newly formed interactions also helped preserve the hydrogel structure of the M-rich alginate at these pHs, although the size of the junction zones increased under these conditions due to the presence of monovalent cations.

These findings offer useful insight into the performance of microcapsules produced from different types of alginate as intestinal-targeted delivery vehicles. Our results showed that G-rich alginates performed better under gastric conditions than M-rich alginates, since their nanostructure was better maintained at pH 3 and even enhanced at lower pH. However, their structural features were also less affected by simulated intestinal conditions, while M-rich capsules completely lost their gel structure at pH ≥ 3. This suggests that the effective release of entrapped bioactive ingredients would be facilitated by high M contents. Further studies should focus on correlating the present structural analysis with the bioaccessibility and bioactivity of encapsulated functional ingredients following simulated gastrointestinal digestion.

Acknowledgements

SAXS experiments were performed at the NCD (Non-Crystalline Diffraction) beamline at ALBA Synchrotron (project 2018022656) with the collaboration of ALBA staff.

DuPont Nutrition & Health is acknowledged for kindly donating the alginate samples for this piece of research. The authors would like to thank the Food Institutional Research Measure (FIRM) initiative of the Irish Department of Agriculture, Food and the Marine for financial support (project 15 F 702).

REFERENCES

Agüero, L., Zaldivar-Silva, D., Pena, L., & Dias, M. L. (2017). Alginate microparticles as oral colon drug delivery device: A review. *Carbohydrate Polymers,* 168, 32-43.

Agulhon, P., Robitzer, M., David, L., & Quignard, F. o. (2011). Structural regime identification in ionotropic alginate gels: influence of the cation nature and alginate structure. *Biomacromolecules,* 13(1), 215-220.

Beaucage, G. (1995). Approximations leading to a unified exponential/power-law approach to small-angle scattering. *Journal of Applied Crystallography,* 28(6), 717-728.

Beaucage, G. (1996). Small-angle scattering from polymeric mass fractals of arbitrary mass-fractal dimension. *Journal of Applied Crystallography,* 29(2), 134-146.

Brodkorb, A., Egger, L., Alminger, M., Alvito, P., Assunção, R., Ballance, S., . . . Recio, I. (2019). INFOGEST static in vitro simulation of gastrointestinal food digestion. *Nature Protocols,* 14(4), 991-1014.

Campos-Vallette, M. M., Chandía, N. P., Clavijo, E., Leal, D., Matsuhiro, B., Osorio-Román, I. O., & Torres, S. (2010). Characterization of sodium alginate and its block fractions by surface-enhanced Raman spectroscopy. *Journal of Raman Spectroscopy,* 41(7), 758-763.

Chan, E.-S., Lee, B.-B., Ravindra, P., & Poncelet, D. (2009). Prediction models for shape and size of ca-alginate macrobeads produced through extrusion–dripping method. *Journal of colloid and interface science,* 338(1), 63-72.

Chuang, J.-J., Huang, Y.-Y., Lo, S.-H., Hsu, T.-F., Huang, W.-Y., Huang, S.-L., & Lin, Y.-S. (2017). Effects of pH on the Shape of Alginate Particles and Its Release Behavior. *International Journal of Polymer Science,* 2017.

Davarcı, F., Turan, D., Ozcelik, B., & Poncelet, D. (2017). The influence of solution viscosities and surface tension on calcium-alginate microbead formation using dripping technique. *Food Hydrocolloids,* 62, 119-127.

de Celis Alonso, B., Rayment, P., Ciampi, E., Ablett, S., Marciani, L., Spiller, R. C., . . . Gowland, P. A. (2010). NMR relaxometry and rheology of ionic and acid alginate gels. *Carbohydrate polymers,* 82(3), 663-669.

Del Gaudio, P., Colombo, P., Colombo, G., Russo, P., & Sonvico, F. (2005). Mechanisms of formation and disintegration of alginate beads obtained by prilling. *International journal of pharmaceutics,* 302(1-2), 1-9.

Draget, K. I., Skjåk-Bræk, G., & Stokke, B. T. (2006). Similarities and differences between alginic acid gels and ionically crosslinked alginate gels. *Food Hydrocolloids,* 20(2-3), 170-175.

Gombotz, W. R., & Wee, S. (1998). Protein release from alginate matrices. *Advanced Drug Delivery Reviews,* 31(3), 267-285.

Gómez-Mascaraque, L. G., Lagarón, J. M., & López-Rubio, A. (2015). Electrosprayed gelatin submicroparticles as edible carriers for the encapsulation of polyphenols of interest in functional foods. *Food Hydrocolloids,* 49(Supplement C), 42-52.

Gómez-Mascaraque, L. G., Llavata-Cabrero, B., Martínez-Sanz, M., Fabra, M. J., & López-Rubio, A. (2018). Self-assembled gelatin-ι-carrageenan encapsulation structures for intestinal-targeted release applications. *Journal of colloid and interface science,* 517, 113-123.
Gómez-Mascaraque, L. G., Soler, C., & Lopez-Rubio, A. (2016). Stability and bioaccessibility of EGCG within edible micro-hydrogels. Chitosan vs. gelatin, a comparative study. *Food Hydrocolloids,* 61, 128-138.
Grant, G. T., Morris, E. R., Rees, D. A., Smith, P. J. C., & Thom, D. (1973). Biological interactions between polysaccharides and divalent cations: The egg-box model. *FEBS Letters,* 32(1), 195-198.
Grasdalen, H., Larsen, B., & Smisrod, O. (1981). 13C-n.m.r. studies of monomeric composition and sequence in alginate. *Carbohydrate Research,* 89(2), 179-191.
Griffin, B. T., Kuentz, M., Vertzoni, M., Kostewicz, E. S., Fei, Y., Faisal, W., . . . Dressman, J. B. (2014). Comparison of in vitro tests at various levels of complexity for the prediction of in vivo performance of lipid-based formulations: Case studies with fenofibrate. *European Journal of Pharmaceutics and Biopharmaceutics,* 86(3), 427-437.
Hecht, H., & Srebnik, S. (2016). Structural characterization of sodium alginate and calcium alginate. *Biomacromolecules,* 17(6), 2160-2167.
Hernández, R., Sacristán, J., & Mijangos, C. (2010). Sol/gel transition of aqueous alginate solutions induced by Fe2+ cations. *Macromolecular Chemistry and Physics,* 211(11), 1254-1260.
Hoad, C., Rayment, P., Cox, E., Wright, P., Butler, M., Spiller, R., & Gowland, P. (2009). Investigation of alginate beads for gastro-intestinal functionality, Part 2: In vivo characterisation. *Food Hydrocolloids,* 23(3), 833-839.
Houghton, D., Wilcox, M. D., Chater, P. I., Brownlee, I. A., Seal, C. J., & Pearson, J. P. (2015). Biological activity of alginate and its effect on pancreatic lipase inhibition as a potential treatment for obesity. *Food Hydrocolloids,* 49, 18-24.
Kendall, W. F., Darrabie, M. D., El-Shewy, H. M., & Opara, E. C. (2004). Effect of alginate composition and purity on alginate microspheres. *Journal of Microencapsulation,* 21(8), 821-828.
Kieffer, J., & Wright, J. (2013). PyFAI: a Python library for high performance azimuthal integration on GPU. *Powder Diffraction,* 28(S2), S339-S350.
Klöck, G., Pfeffermann, A., Ryser, C., Gröhn, P., Kuttler, B., Hahn, H.-J., & Zimmermann, U. (1997). Biocompatibility of mannuronic acid-rich alginates. *Biomaterials,* 18(10), 707-713.
Kristiansen, K. A., Tomren, H. B., & Christensen, B. E. (2011). Periodate oxidized alginates: Depolymerization kinetics. *Carbohydrate polymers,* 86(4), 1595-1601.
LeRoux, M. A., Guilak, F., & Setton, L. A. (1999). Compressive and shear properties of alginate gel: effects of sodium ions and alginate concentration. *Journal of Biomedical Materials Research: An Official Journal of The Society for Biomaterials, The Japanese Society for Biomaterials, and The Australian Society for Biomaterials and the Korean Society for Biomaterials,* 47(1), 46-53.
Martínez-Sanz, M., Gómez-Mascaraque, L. G., Ballester, A. R., Martínez-Abad, A., Brodkorb, A., & López-Rubio, A. (2019). Production of unpurified agar-based extracts from red seaweed Gelidium sesquipedale by means of simplified extraction protocols. *Algal Research,* 38, 101420.
Minekus, M., Alminger, M., Alvito, P., Ballance, S., Bohn, T., Bourlieu, C., . . . Dupont, D. (2014). A standardised static in vitro digestion method suitable for food–an international consensus. *Food & function,* 5(6), 1113-1124.
Mulet-Cabero, A.-I., Mackie, A., Wilde, P., Fenelon, M. A., & Brodkorb, A. (2019). Structural mechanism and kinetics of in vitro gastric digestion are affected by process-induced changes in bovine milk. *Food Hydrocolloids,* 86, 172-183.

Mulet-Cabero, A.-I., Rigby, N. M., Brodkorb, A., & Mackie, A. R. (2017). Dairy food structures influence the rates of nutrient digestion through different in vitro gastric behaviour. *Food Hydrocolloids,* 67, 63-73.

Oomen, A. G., Rompelberg, C. J. M., Bruil, M. A., Dobbe, C. J. G., Pereboom, D. P. K. H., & Sips, A. J. A. M. (2003). Development of an In Vitro Digestion Model for Estimating the Bioaccessibility of Soil Contaminants. *Archives of Environmental Contamination and Toxicology,* 44(3), 0281-0287.

Ozen, A. E., Pons, A., & Tur, J. A. (2012). Worldwide consumption of functional foods: a systematic review. *Nutrition reviews,* 70(8), 472-481.

Qi, X., & Tester, R. F. (2019). Utilisation of dietary fibre (non-starch polysaccharide and resistant starch) molecules for diarrhoea therapy: A mini-review. *International Journal of Biological Macromolecules,* 122, 572-577.

Ramos, P. E., Silva, P., Alario, M. M., Pastrana, L. M., Teixeira, J. A., Cerqueira, M. A., & Vicente, A. A. (2018). Effect of alginate molecular weight and M/G ratio in beads properties foreseeing the protection of probiotics. *Food Hydrocolloids,* 77, 8-16.

Rayment, P., Wright, P., Hoad, C., Ciampi, E., Haydock, D., Gowland, P., & Butler, M. F. (2009). Investigation of alginate beads for gastro-intestinal functionality, Part 1: In vitro characterisation. *Food Hydrocolloids,* 23(3), 816-822.

Rioux, L.-E., & Turgeon, S. L. (2015). *Seaweed carbohydrates*. In *Seaweed Sustainability* (pp. 141-192): Elsevier

Salomonsen, T., Jensen, H. M., Stenbæk, D., & Engelsen, S. B. (2008). Chemometric prediction of alginate monomer composition: A comparative spectroscopic study using IR, Raman, NIR and NMR. *Carbohydrate Polymers,* 72(4), 730-739.

Schuster, E., Wallin, P., Klose, F., Gold, J., & Ström, A. (2017). Correlating network structure with functional properties of capillary alginate gels for muscle fiber formation. *Food Hydrocolloids,* 72, 210-218.

Shani-Levi, C., Alvito, P., Andrés, A., Assunção, R., Barberá, R., Blanquet-Diot, S., . . . Deglaire, A. (2017). Extending in vitro digestion models to specific human populations: Perspectives, practical tools and bio-relevant information. *Trends in food science & technology,* 60, 52-63.

Simpson, N. E., Stabler, C. L., Simpson, C. P., Sambanis, A., & Constantinidis, I. (2004). The role of the $CaCl_2$–guluronic acid interaction on alginate encapsulated βTC3 cells. *Biomaterials,* 25(13), 2603-2610.

Smidsrød, O. (1974). Molecular basis for some physical properties of alginates in the gel state. *Faraday discussions of the Chemical Society,* 57, 263-274.

Strobel, S. A., Scher, H. B., Nitin, N., & Jeoh, T. (2016). In situ cross-linking of alginate during spray-drying to microencapsulate lipids in powder. *Food Hydrocolloids,* 58, 141-149.

Versantvoort, C. H., Oomen, A. G., Van de Kamp, E., Rompelberg, C. J., & Sips, A. J. (2005). Applicability of an in vitro digestion model in assessing the bioaccessibility of mycotoxins from food. *Food and Chemical Toxicology,* 43(1), 31-40.

Wilcox, M. D., Brownlee, I. A., Richardson, J. C., Dettmar, P. W., & Pearson, J. P. (2014). The modulation of pancreatic lipase activity by alginates. *Food chemistry,* 146, 479-484.